metals

Article

The Effects of Recrystallization on Strength and Impact Toughness of Cold-Worked High-Mn Austenitic Steels

Minha Park [1,2], Moon Seok Kang [1,2], Geon-Woo Park [1], Eun Young Choi [1], Hyoung-Chan Kim [1], Hyoung-Seok Moon [1], Jong Bae Jeon [1], Hyunmyung Kim [3], Se-Hun Kwon [2,*] and Byung Jun Kim [1,*]

[1] Dongnam Regional Division, Korea Institute of Industrial Technology, Busan 46938, Korea
[2] School of Materials Science and Engineering, Pusan National University, Busan 46241, Korea
[3] Korea National Ppuri Industry Center, Korea Institute of Industrial Technology, Seoul 06211, Korea
* Correspondence: jun7741@kitech.re.kr (B.J.K.); sehun@pusan.ac.kr (S.-H.K.); Tel.: +82-10-5136-7743 (B.J.K.); +82-10-3364-0617 (S.-H.K.)

Received: 2 August 2019; Accepted: 28 August 2019; Published: 29 August 2019

Abstract: High-Mn austenitic steels have been recently developed for a storage or transportation application of liquefied natural gas (LNG) in cryogenic fields. Since the structural materials are subjected to extremely low temperature, it requires excellent mechanical properties such as high toughness strength. In case of high-Mn steels, twinning deformation during the cold-working process is known to increase strength yet may cause embrittlement of heavy deformed twin and anisotropic properties. In this study, a recrystallization process through appropriate annealing heat treatments after cold-working was applied to improve the impact toughness for high-Mn austenitic steels. Microstructure and mechanical properties were performed to evaluate the influence of cold-worked and annealed high-Mn austenitic steels. Mechanical properties, such as strength and impact toughness, were investigated by tensile and Charpy impact tests. The relationship between strength and impact toughness was determined by microstructure analysis such as the degree of recrystallization and grain refinement. Consequently, both elongation and toughness were significantly increased after cold-working and subsequent annealing at 1000 °C as compared to the as-received (hot-rolled) specimen. The cold-worked high-Mn steel was completely recrystallized at 1000 °C and showed a homogeneous micro-structure with high-angle grain boundaries.

Keywords: high-Mn steel; cold-working; annealing; recrystallization; twinning

1. Introduction

As the demand for cryogenic industries such as liquefied natural gas (LNG) has increased in the last few years, the materials for storage and application of cryogenics have become more important [1,2]. Generally, materials with face-centered cubic (FCC) structures such as austenitic stainless steels, like 9 wt% Ni-steels with the addition of Al and Ti elements, are widely used in cryogenic fields because of their good mechanical properties at cryogenic temperature [3–5]. Yet, these materials have disadvantages, such as costly products, difficult processing, low design strength and complicated manufacturing. Therefore, high-Mn austenitic steels containing over 24 wt% of Mn with excellent mechanical properties in a cryogenic environment have been newly developed to replace the existing cryogenic materials [6].

The high-Mn austenitic steels show a fully austenite phase at room temperature and have good mechanical properties by deformation mechanisms at low temperatures [7]. These steels demonstrate mechanical twinning instead of phase transformation to martensite after plastic deformation, which is called twinning-induced plasticity (TWIP) [8]. These mechanisms depend on stacking fault energy (SFE), and the SFE generally increases as Mn, Cr and Ni content increase in TWIP steels. TWIP effects are activated in the SFE range of 20–40 mJ/m^2 [9,10], and strength resultantly is enhanced by the formation of mechanical twinning induced with cold plastic working [11,12]. The high work-hardening is generally caused by reduction in dislocation mean free path with an increasing fractions of deformation twinning acting as strong obstacles to the dislocation glide [13]. Nucleation of deformation twining occurs by interaction of dislocation structure and the twin boundary [14,15]. The strength and toughness can be simultaneously improved by an appropriate twinning effect. Thus, it isvery important to understand the effects of microstructure and mechanical properties of twinning in TWIP steels [16,17].

In general, grain size refinement is an important mechanism for strengthening and toughening, especially for high-Mn steels [18–21]. The recrystallization annealing combined with cold-working is a very effective approach for the austenite grain size refinement, as many components used in cryogenic environments are produced. The mechanical properties of cold-worked high-Mn steels can be improved by subsequent annealing [22–25] as dislocation and the twin boundary act as nucleation sites for recrystallization during annealing [26,27]. As the annealing temperature is increased, ductility and toughness is improved by a recrystallized microstructure with grain refinement. Grain refinement and recrystallization are affected by various conditions such as rolling reduction, annealing temperature, compositions of alloying element [28,29]. Especially, it was reported that recrystallization of austenitic high-Mn steels containing over 20 wt% of Mn started at temperatures around 600 °C [30]. Also, the increase in deformation by cold rolling accelerated the recrystallization kinetics and produced the effect of refining recrystallized grains. Therefore, the thermo-mechanical processing of grain refinement using cold rolling and annealing is an effective way to improve the mechanical properties of high-Mn steels.

In order to study the mechanical properties during work hardening and annealing, it isvery important to understand the deformed microstructure such as misorientation and grain boundary properties. Low angle grain boundaries (LAGBs) and high angle grain boundaries (HAGBs) are often defined with a misorientation angle of $2° < \theta < 15°$ and $15° < \theta$, respectively. The volume fraction of LAGBs in deformed samples means the formation of a deformed microstructure and dislocations. On the other hand, the grains after annealing have a lower volume fraction of LAGBs compared to the deformed grains because of lower internal misorientation by annihilation of dislocation. When considering the toughness of the steels, LAGBs are known to be less effective in impeding crack growth than HAGBs. In other words, recrystallized microstructure after annealing consists of larger volume fractions of HAGBs than LAGBs. In addition to the recrystallization, annealing heat treatments decrease the deformation twins by the grain growth while increase annealing twins [31] in which the annealing twin generated in the heat treatment causes grain refinement effect by grain subdivision.

In this study, the degree of cold-working and subsequent annealing on microstructure and mechanical properties were investigated in relation to recrystallization and grain refinement in high-Mn steels. For cryogenic applications, the improvement of impact toughness is important to ensure the safety and integrity of structural materials because strength increases at low temperatures [32,33]. Therefore, our study focuses on the improvement of impact toughness and investigates the correlation between microstructural changes and mechanical properties by heat treatment to determine to improve strength and ductility.

2. Materials and Methods

The chemical compositions of the high-Mn steels used in this study are shown in Table 1. A plate with a width 1500 mm, length of 200 mm, and thickness of 20 mm was fabricated by the hot rolling process.

Table 1. Chemical compositions of high-Mn austenitic steels used in this study (wt%).

C	Mn	Si	Cr	P	S	Cu	Fe
0.44	24	0.27	3.4	0.013	0.0023	0.429	Bal.

From the as-received (AS) high-Mn steels, a plate of steel with 20 mm thickness was cold-worked into different thicknesses of the plates CW5, CW10, and CW30, with reductions of plate thickness by 5%, 10%, and 30%, respectively. In order to recrystallize high-Mn steel, the cold-worked samples were annealed at various temperature from 600 to 1000 °C for 15 min and followed by water quenching. Schematic diagram of annealing process and specimen direction for high-Mn austenitic steels in this study was shown in Figure 1.

For the microstructure analysis, the test samples were mechanically polished using a 320, 600, 1200, 2000 grit SiC paper and then micro-polished using a 3 and 1 μm diamond paste. Then, sample surfaces of cold-worked samples were etched in a solution contacting 100 mL ethanol, 1g picric acid, 5ml hydrochloric (Vilella's reagent) and annealed samples were etched with 3% Nital solution respectively. The microstructures of the cold-worked and annealed specimens were observed using optical microscopy (OM). The average grain size of annealed specimens was evaluated by image analysis, using the intercept method on the OM images.

The X-ray diffraction (XRD) patterns of the cold-worked and annealed specimens were measured at room temperature in the range of 20–100° for 2θ degree with Cu Kα radiation. The phase was identified by X'pert Pro XRD machine with a speed of 0.013 degree per second. The (111), (200), (220), (311) and (222) peaks were used to observe austenite phases.

Tensile testing was carried out at room temperature using a 100 kN full-automatic MTS E45 tensile machine at a cross head speed of 1 mm/min. The dimensions of the plate-type sub-sized tensile specimens were 25 mm in gauge length, 6 mm in width, and 2 mm in thickness in ASTM-E8. The 0.2% offset stress was determined to be the yield strength in the specimens showing continuous yielding behavior and the elongation determined by the travel distance of crosshead.

Vickers hardness tests were performed at room temperature with a load of 4.903 N with 10 s of dwell time. At least seven measurements were made to calculate the average micro-hardness values by excluding the minimum value and maximum value.

Charpy V-notch impact tests were performed to measure the absorbed energy at temperatures from 20 °C to −180 °C using a full-automatic ZWIC impact test machine according (Zwick) to ASTM E23. The geometry of the standard sized Charpy V-notched specimen measures 10 mm (width), 10 mm (height) and 55 mm (length). The fracture surface of the Charpy impact test specimen was observed with a FE-SEM HITACHI S-4800 (HITACHI, Tokyo, Japan)

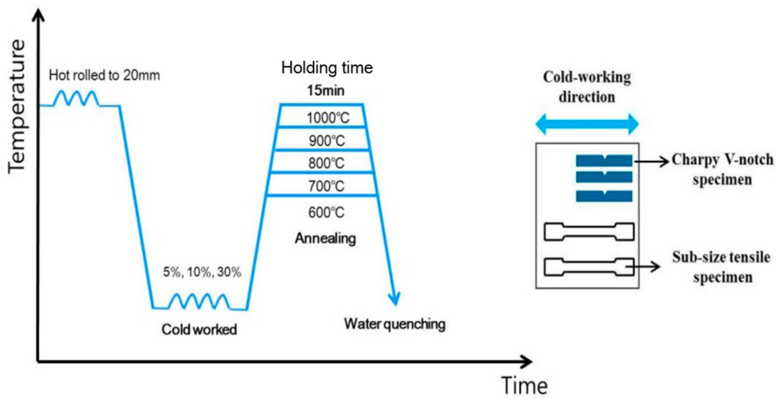

Figure 1. Schematic diagram of annealing process and specimen direction for high-Mn austenitic steels in this study.

Electron backscattered diffraction (EBSD) was carried out using JEOL FE-SEM 7200F with Oxford software. The grain boundary distributions were obtained to determine the recrystallization behavior. LAGBs were defined as the misorientation angles ranging from 2° to 15°, and HAGBs were defined as the misorientation angles higher than 15°. Misorientation angle distributions of different annealing conditions were obtained to discuss the relationship between microstructure and mechanical properties. The EBSD measurements were operated at a voltage of 20 kV.

3. Results and Discussion

3.1. Microstructure Analysis of Cold-Worked High-Mn Steels

Figure 2 shows the optical microstructure of high-Mn Austenitic steels before and after a cold-working process. The microstructure of as-received sample was typically a hot-rolled austenitic structure consisted of austenite single phase and hot-rolling strips. These rolling strips were elongated in the same direction as the grain boundaries drawn in the hot rolling direction, as shown in Figure 2a. After the cold-working process, deformation twin and slip bands were observed inside grains in Figure 2b–d while deformation twinning increased with an increase in the cold-working level from 5% to 30% [8]. Therefore, the cold-working process induced deformation twinning in the austenite grains, and the density of twinning increases with increasing cold-working reduction leading to grain subdivision.

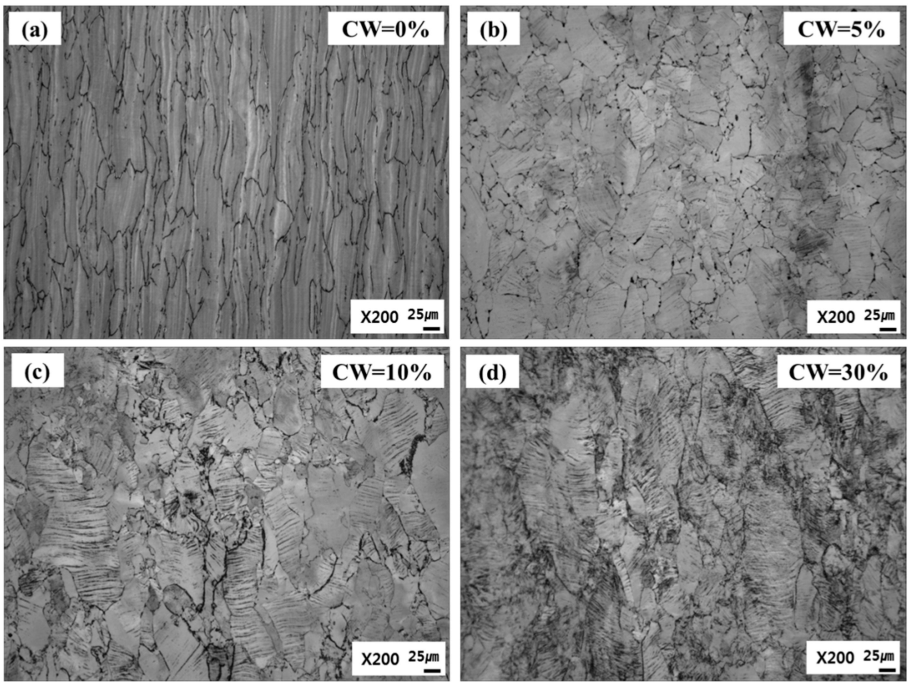

Figure 2. Optical microstructure of high-Mn Austenitic steels before and after a cold-working process (**a**) as-received, (**b**) 5% CW, (**c**) 10% CW and (**d**) 30% CW.

Figure 3 shows the optical microstructure of cold-worked high-Mn steels after annealing at different temperatures and degree of recrystallization. The typical partially recrystallized microstructure observed around grain boundary at 600 °C. A number of the fine recrystallized grains increased with the cold-working level from 5% to 30% in Figure 2a,d. Deformation twins were still present in the grain boundaries at which recrystallization did not occur even after the annealing at 600 °C. It has been recently studied that the twins generated by deformation at room temperature are stable up to a temperature of 625 °C [34]. A lot of recrystallization was observed in 30% cold-worked specimens than in other specimens because the nucleation site is increased and the recrystallization temperature was lowered after cold-working process. Also, the driving force for recrystallization became larger from the stored energy of increased cold-working level. The prior cold-working introduces a high density of dislocation [35], which transforms into polygonised subgrains upon heating to the processing temperature [14]. In the case of annealing at 800 °C, grain boundaries refinement was more observed in a 30% cold-worked specimen than in the other cold-worked conditions. In case of annealing at 1000 °C, fine recrystallized grains grew and became homogeneous austenitic structure with annealing twin.

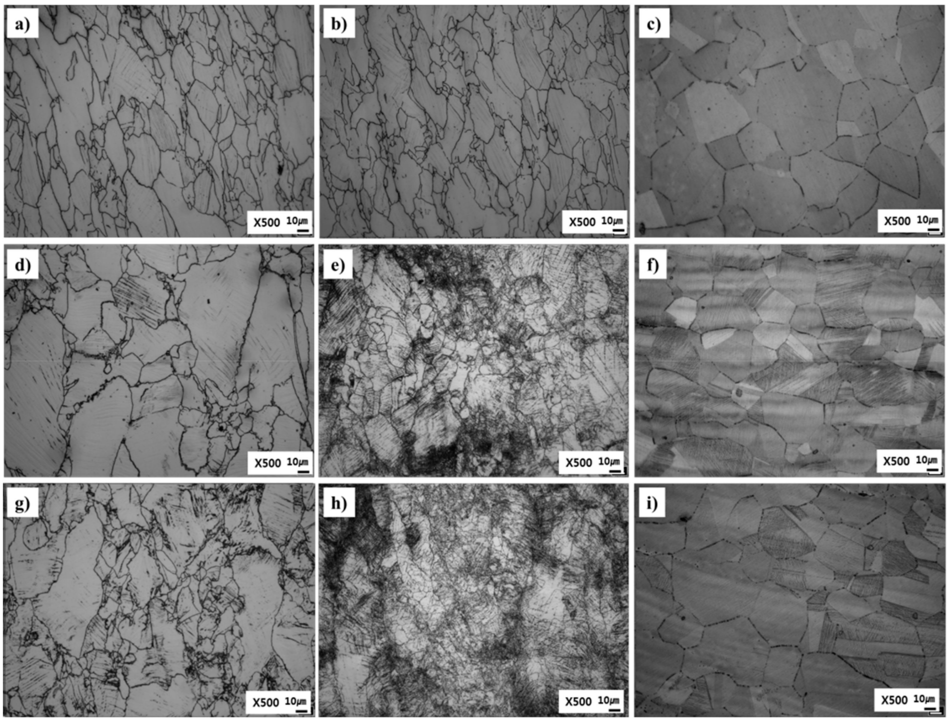

Figure 3. Optical microstructures of cold-worked high-Mn steels after annealing. (**a**) CW5_H600, (**b**) CW5_H800, (**c**) CW5_H1000, (**d**) CW10_H600, (**e**) CW10_H800, (**f**) CW10_H1000, (**g**) CW30_H600, (**h**) CW30_H800, and (**i**) CW30_H1000.

Figure 4 shows the average grain size of cold-worked high-Mn steels after annealing. The average grain size of the as-received specimen was measured to be about 47 µm and the average grain size after the annealing at 1000 °C was significantly reduced to less than about 23 µm. After the annealing at 1000 °C, there was no significant difference in the grain size according to the cold-working level from 5% to 30%. The grain refinement by annealing is caused by the recrystallization and grain subdivision by annealing twin.

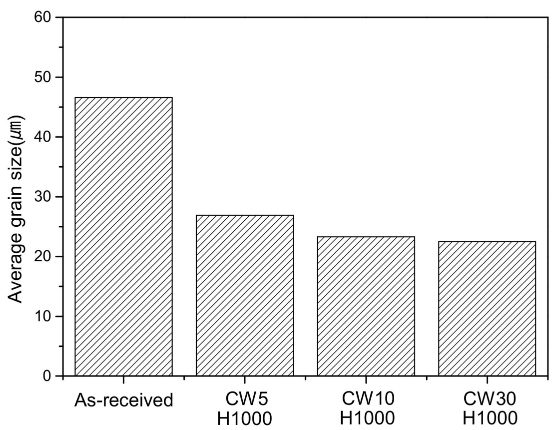

Figure 4. The average grain size of cold-worked high-Mn steels after annealing.

Figure 5 shows an EBSD inverse pole figure (IPF) map with grain boundaries of 30% cold-worked steels after annealing from 600 °C to 1000 °C. The microstructure of the 30% cold-worked specimen (CW30) is mostly elongated austenitic grains due to the deformation caused by the cold-working process (Figure 5a). In case of annealing at 600 °C, the microstructure exhibits heterogeneous structures which have fine recrystallized grains and non-recrystallized grains (Figure 5b). In case of annealing at 800 °C, most of the grain boundaries were observed to have a grain refinement by recrystallization. However, the recrystallization was not completed yet, and it still had a heterogeneous structures. In case of annealing at 1000 °C, the microstructure shows fully austenite structure with homogeneous recrystallized grains (Figure 5d).

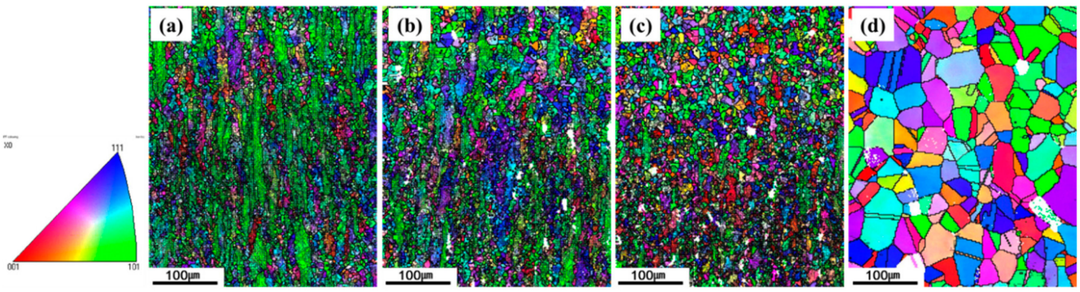

Figure 5. EBSD inverse pole figure (IPF) map of 30% cold-worked high-Mn steels after annealing: (**a**) CW30, (**b**) CW30_H600, (**c**) CW30_H800 and (**d**) CW30_H1000.

Figure 6 shows the misorientation angle distribution and Σ3 grain boundary distribution of 30% cold-worked steels after annealing from 600 °C to 1000 °C. In the grain boundary maps, low angle grain boundaries(LAGBs) with 2° < θ < 15°, high angle grain boundaries (HAGBs) with θ > 15° are drawn in Figure 6a. The fraction of LAGBs and HAGBs for 30% cold-worked steels (CW30) are 52.8% and 45.3%, respectively, while the value for annealed specimens at 1000 (CW30_H1000) are 3% and 95.2%, respectively. As the annealing temperature increased, the fraction of LAGBs decreased and the fraction of HAGBs increased. It is indicate that austenite structure with LAGBs is transformed into austenite structure with HAGBs after annealing. The relative frequency of coincidence site lattice (CSL) Σ3 which is defined as a twin boundary was maintained at 800 °C, but it was significantly increased above 800 °C (Figure 6b). Especially, the relative frequency of CSL for annealed specimens at 1000 °C (CW30_H1000) increased about three times compared to the 30% cold-worked specimen (CW30). As a result of the average grain size (Figure 4), the annealing twins produced by recrystallization contribute to the grain refinement by grain subdivision.

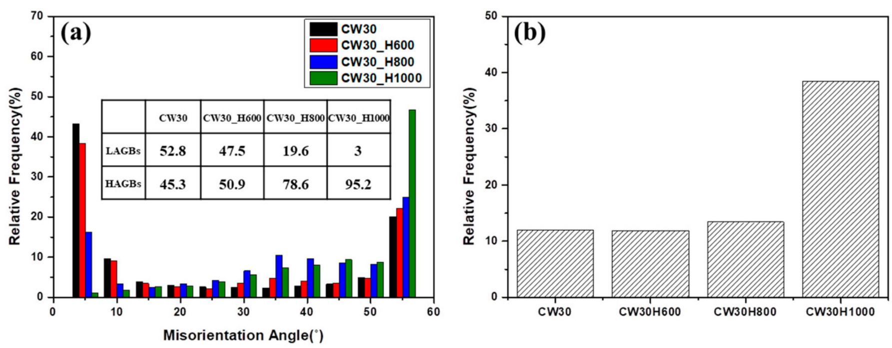

Figure 6. Misorientation angle distribution (**a**) and frequency of Σ3 grain boundary (**b**) in the 30% cold-worked high-Mn steels after annealing.

Figure 7 shows the XRD patterns of cold-worked high-Mn Austenitic steels before and after annealing. Before and after a cold-working process, only austenite peaks were observed in all conditions (Figure 7a). TWIP mechanism activates in the SFE range from 20 to 40 mJ/m^2, whereas decreasing the SFE from 20 to 12 mJ/m^2 results in improving the ductility of the steel by the transformation-induced plasticity (TRIP) effect. According to the composition-temperature-related equations proposed by Curtze et al. [10], the room temperature SFE is calculated to be 29 mJ/m^2 for 24Mn steels in this study. Also, since the SFE of the high manganese steel was 20 or more even after annealing, only peaks of austenite was observed in Figure 7b. It is indicated that work hardening by a cold-working process is not induced by TRIP effects but twinning mechanism of deformation.

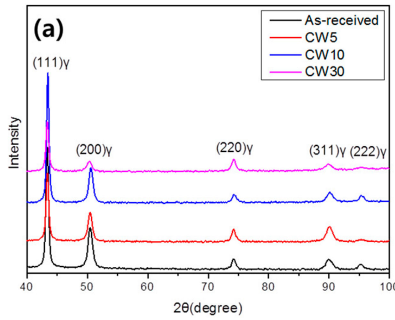

Figure 7. XRD patterns of cold-worked high-Mn Austenitic steels (**a**) before and (**b**) after annealing.

3.2. Tensile and Hardness Properties of Cold-Worked High-Mn Steels

The engineering stress–strain curves obtained by tensile tests for the high-Mn austenitic steels before and after a cold-working process are shown in Figure 8a. The ultimate tensile strength of highly cold-worked steel (CW30) was about 1.5 times higher than that of the as-received steels (AS). The tensile strength and yield strength (0.2% offset) gradually increased with an increase of the cold-working level from 5% to 30%. This behavior was attributed to the strain hardening owing to the interaction among dislocation and twin generated by the cold-working process. However, the elongation of cold-worked steels decreased due to a increase in dislocations density [22]. Especially, the strengthening in cold-worked high-Mn steel was increased by twinning mechanism and increase in dislocations density [22,36]. As shown in the EBSD analysis results (Figure 5), misorientation distribution of cold-worked high-Mn austenitic steels have characterized as LABGs, resulting in increased strength and decreased ductility.

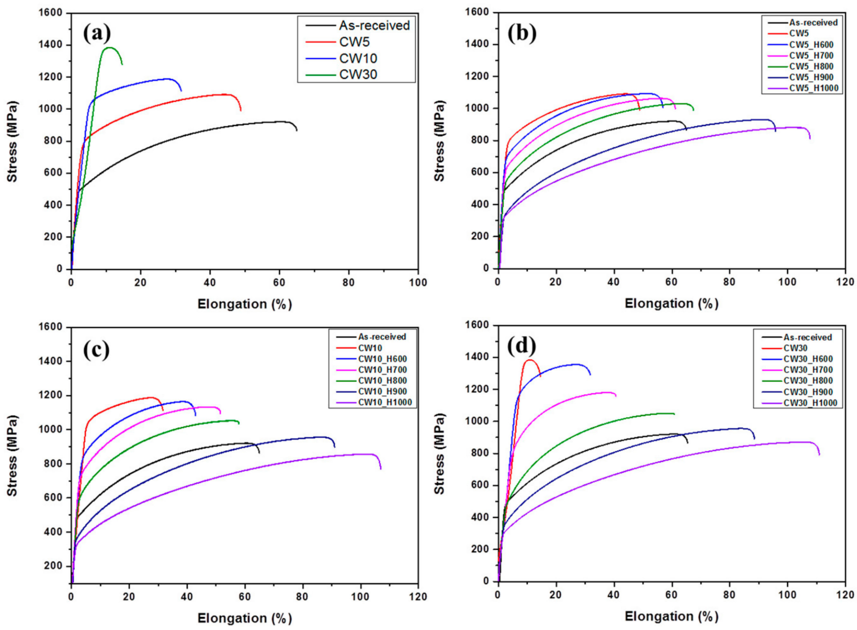

Figure 8. The engineering stress–strain curves of cold-worked high-Mn steels before and after annealing: (**a**) before annealing, (**b**) CW5, (**c**) CW10 and (**d**) CW30.

The engineering stress–strain curves for the cold-worked high-Mn steels after annealing are shown in Figure 8b–d. Tensile strength and yield strength decreased with increasing annealing temperature from 600 °C to 1000 °C, but the elongation increased. In particular, the elongation of the highly cold-worked specimen after annealing significantly increased from 15% (CW30) to 110% (CW30_H1000) and increased by about 83% compared with as-received specimen (AS). The tensile properties of annealed specimens at 800 °C were different from those of as-received specimen. As previously shown in the microstructure analysis results (Figure 3b,e,h), the microstructure was not completely recrystallized nor homogenized below 800 °C. In addition, ductility was not recovered due to the still presence of mechanical twin within the grains. However, the elongation at temperatures above 800 °C has higher than that of the as-received specimen. At annealing temperatures above 800 °C, the austenitic grain with homogeneous microstructure was completely recrystallized, and the ductility was improved by grain refinement induced by annealing twin and recrystallization. Such recrystallization microstructure changed from LAGBs to HAGBs improved ductility with increasing annealing temperature (Figure 6a). The tensile properties did not depend on the cold-working level due to the completely recrystallized new grains at 1000 °C.

Figure 9 shows the result of the Vickers hardness test before and after a cold-working process. The hardness value of as-received steel (AS) was about 280HV. Similar to the tensile test results, the hardness values increased in the degree of cold-working. The hardness value of highly cold-worked steel (CW30) with a reduction of plate thickness by 30% was about 86% higher than that of the as-received steels (AS). The increase of hardness values after cold-working process was resulted from the same mechanism as that in the tensile results, owing to the deformation twinning and increased dislocation density. The hardness of the cold-worked specimens after annealing decreased with increasing annealing temperature. At temperatures below 700 °C, hardness values differ according to the cold-working level. Below 800 °C, the grains were not completely recrystallized despite annealing, which maintained high twinning and high dislocation density. In addition, the microstructure had a mixture of twinned deformed grains and dislocations-free recovered grains for cold-working specimens. However, hardness values do not depend on the cold-working level since the dislocation density and twinning were almost recovered above 800 °C. Likewise, the hot-rolling strips and high dislocation density existing in the as-received specimen were also recovered after annealing above 800 °C. Mechanical properties such as the test results of the tensile properties and Vickers hardness values are summarized in Table 2.

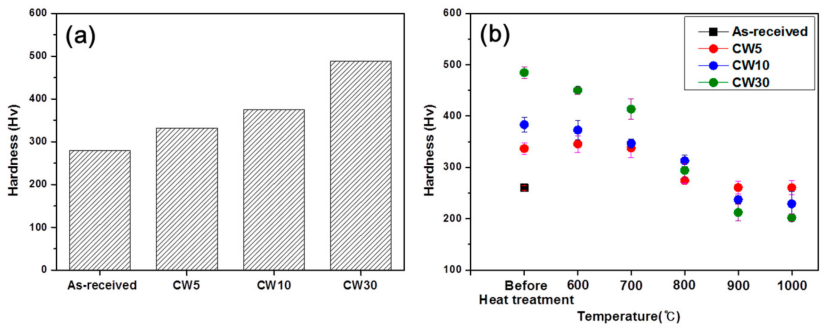

Figure 9. Hardness of cold-worked high-Mn steels before and after annealing. (**a**) Before annealing, (**b**) after annealing.

Table 2. Tensile properties and Vickers hardness values of the specimens used in this study.

Specimen ID	Yield Strength (MPa)	Tensile Strength (MPa)	Elongation (%)	Average Vickers Hardness (Hv)
As-received	486	920	83	259
CW5	791	1091	49	336
CW5_H600	690	1093	57	345
CW5_H700	603	1063	61	337
CW5_H800	524	1030	67	274
CW5_H900	322	931	96	260
CW5_H1000	318	881	107	260
CW10	1042	1187	31	383
CW10_H600	834	1164	43	372
CW10_H700	721	1133	51	346
CW10_H800	571	1052	58	312
CW10_H900	346	956	90	237
CW10_H1000	338	856	107	228
CW30	1365	1384	15	484
CW30_H600	1149	1355	31	449
CW30_H700	846	1179	40	413
CW30_H800	498	1051	60	293
CW30_H900	362	955	88	212
CW30_H1000	311	870	110	201

3.3. Impact Toughness of Cold-Worked High-Mn Steels

The absorbed energy vs. test temperature curves for specimens with a cold-working process is shown in Figure 10a. At room temperature, the absorbed energy of as-received specimens was about 120 J. Although high-Mn Austenitic steels with face centered cubic (FCC) structure does not show the ductile-to-brittle temperature (DBTT) behavior, the absorbed energy tends to decrease with decreasing temperature. The absorbed energy of cold-worked steels decreased with the cold-working level from 5% to 30%. High-Mn steels after a cold-working process generally resulted in a higher yield strength and lower ductility due to the increase in dislocation density and deformation twinning. Therefore, the result of the Charpy impact test provided the decrease in absorbed energy due to the reduction of ductility by a cold-working process.

The absorbed energy vs. test temperature curves for cold-worked specimens after annealing are shown in Figure 10b–d. At annealing range from 600 to 800 °C, the absorbed energy was lower than that of the as-received steel due to the heterogeneous microstructure by incomplete recrystallization and the remaining twinning and high dislocation density. However, the absorbed energy was higher than that of the as-received steel at annealing temperatures above 800 °C. Especially at 1000 °C, the absorbed energy increased about two times comparing the as-received steels regardless of the cold-working level. Figure 11 shows EBSD grain boundary maps of as-received and 30% cold-worked specimen after annealing (1000 °C). Low angle grain boundaries (LAGBs) and high angle grain boundaries (HAGBs) are plotted by red lines and black lines, respectively. For the as-received state, the austenitic grains with diameter about 47 µm (Figure 4) have some of LAGBs, shown in Figure 11a. However, for the 30% cold-worked specimen after annealing (1000 °C), the fully recrystallized microstructure shows coarse equiaxed grains with diameter about 27 µm (Figure 4) and there are few of LAGBs than as-received samples, as observed in Figure 11b. In addition, microstructure was changed from LAGBs to HAGBs by recrystallization and grain growth after annealing process. In particular, grain refinement occurred due to recrystallization and grain subdivision by the annealing twins. For the reasons such as HAGBs and grain refinement, the improvement of impact toughness is due to an increase in energy consumption by cracks through the grain boundary [37]. Therefore, the absorbed energy of the 30% cold-worked specimen after annealing (1000 °C) was significantly increased due to a homogeneous microstructure with HAGBs and grain refinement by complete recrystallization at 1000 °C.

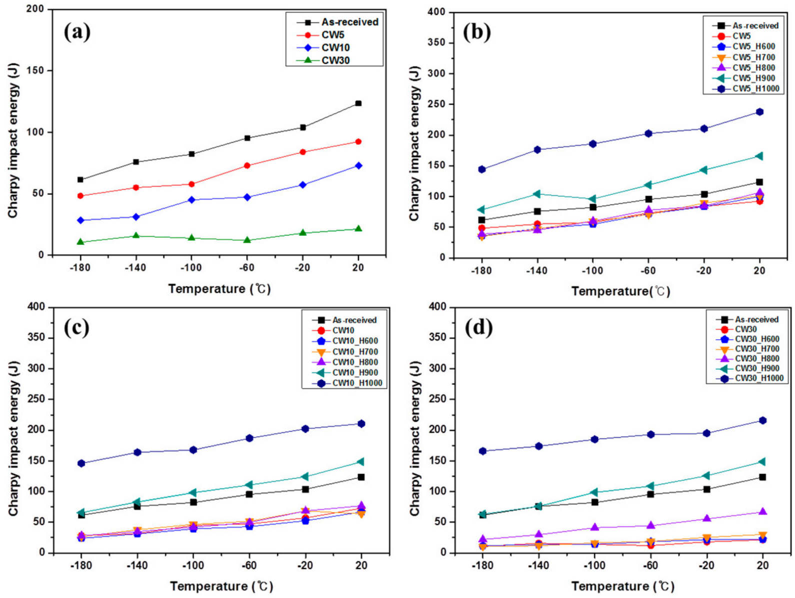

Figure 10. The absorbed energy vs. test temperature curves of cold-worked high-Mn steels after annealing. (**a**) Before annealing, (**b**) CW5, (**c**) CW10 and (**d**) CW30.

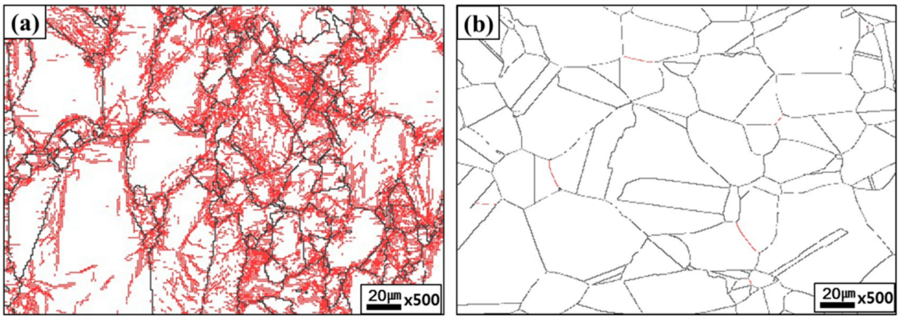

Figure 11. EBSD grain boundary maps of (**a**) as-received and (**b**) CW30_H1000. The LAGBs, HAGBs, boundaries are plotted as red lines, black lines, respectively.

Figure 12 shows the fracture surface of cold-worked high-Mn steels before/after annealing (1000 °C) at cryogenic temperature (−180 °C). The fracture surface of the as-received specimen showed mostly quasi-brittle fracture mode and partially ductile mode including dimples (Figure 12a). The cold-worked specimens were fractured without plastic deformation; the quasi-brittle fracture mode was mostly observed in the fracture surface (Figure 12b–d). The fracture surfaces of annealed specimens (1000 °C) mostly show ductile fracture modes including many small dimples and partially quasi-brittle fracture mode (Figure 12e–g). There was no significant difference in the fracture surface depending on the annealing temperature. The shape of the fractured specimen after annealing shows severe plastic deformation compared to that of the as-received specimen. The results of fracture surface analysis were in good agreement with the results of the absorbed energy from the Charpy impact test at cryogenic temperature.

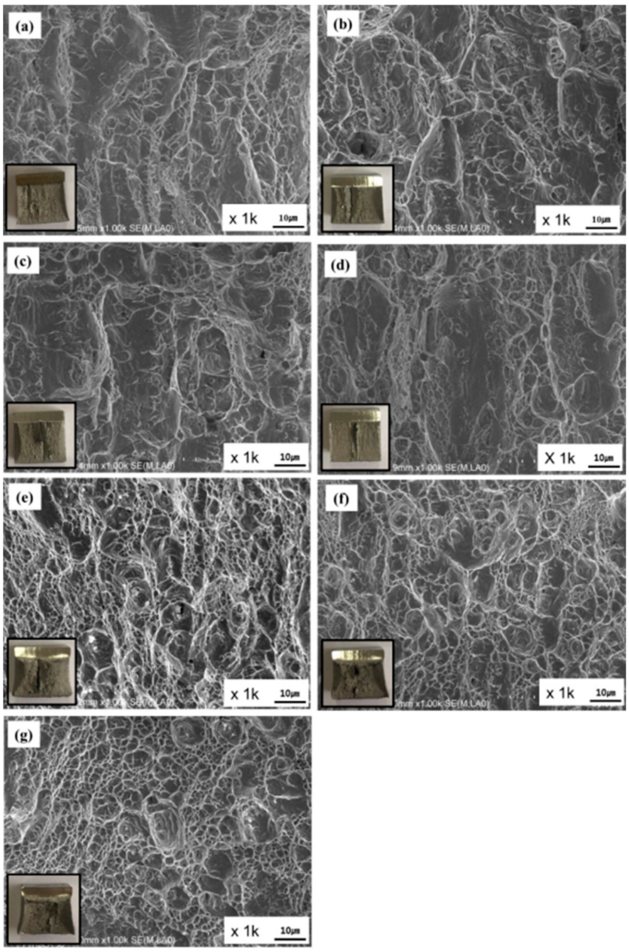

Figure 12. The fracture surface of cold-worked high-Mn steels before/after annealing (1000 °C) at cryogenic temperature (−180 °C): (**a**) as-received, (**b**) CW5, (**c**) CW10, (**d**) CW30, (**e**) CW5_H1000, (**f**) CW10_H1000 and (**g**) CW30_H1000.

4. Conclusions

In this study, we investigate the effects of recrystallization on strength and impact toughness of cold-worked and subsequently annealed high-Mn austenitic steels.

1. Microstructures of as-received exhibited elongated austenite grains and the cold-worked high-Mn austenitic steels reveal deformation twinning in the grains. The microstructure of annealed specimens below 800 °C exhibits heterogeneous microstructure which have partially recrystallization region with a high volume fraction of LAGBs, whereas the microstructure of annealed specimens over 800 °C shows homogeneous microstructure which have fully austenite structure with HAGBs.
2. The average grain size of the as-received specimen was measured to be about 47 μm and the average grain size after the annealing at 1000 °C was significantly reduced to less than about 23 μm. The grain refinement after the annealing is caused by the recrystallization and grain subdivision by annealing twin.
3. The tensile strength and yield strength of cold-worked steels increased with an increase of the cold-working level from 5% to 30% due to the deformation twinning and high volume fraction of LAGBs. At an annealing temperature above 800 °C, the austenite grain was completely recrystallized, and the elongation was improved by grain refinement induced by annealing twin and homogeneous microstructure with HAGBs.

4. The absorbed energy of cold-worked steels decreased with the cold-working level from 5% to 30%. After annealing, the absorbed energy increased with increasing annealing temperature. Especially at 1000 °C, the absorbed energy increased about two times comparing the as-received steels regardless of the cold-working level. It was found that the increase in impact toughness after annealing is due to homogeneous microstructure with HAGBs and grain refinement by complete recrystallization. In addition, the results of fracture surface analysis were in good agreement with the results of the absorbed energy from the Charpy impact test at cryogenic temperature.

Author Contributions: M.P. and B.J.K. conceived and designed the experiments; M.P. and M.S.K. performed the experiments; G.W.P., E.Y.C., H.C.K., H.-S.M., J.B.J., H.K., S.-H.K. and B.J.K. analyzed and discussed the data; M.P. and B.J.K. wrote the paper;

Acknowledgments: This study was supported by the R&D Program of the Korea Evaluation Institute of Industrial Technology (KEIT) as "Development of Sub-merged-Arc-Welded Pipe and Extruded Pipe made of High Manganese Steel for Cryogenic Usage in LNG Ship and Offshore Plant" (10080728).

Conflicts of Interest: The authors declare no conflict of interest.

References

1. Kumar, S.; Kwon, H.-T.; Choi, K.-H.; Lim, W.; Cho, J.H.; Tak, K.; Moon, I. LNG: An eco-friendly cryogenic fuel for sustainable development. *Appl. Energy* **2011**, *88*, 4264–4273. [CrossRef]
2. Kumar, S.; Kwon, H.-T.; Choi, K.-H.; Cho, J.H.; Lim, W.; Moon, I. Current status and future projections of LNG demand and supplies: A global prospective. *Energy Policy* **2011**, *39*, 4097–4104. [CrossRef]
3. Baek, J.-H.; Kim, Y.-P.; Kim, W.-S.; Kho, Y.-T. Fracture toughness and fatigue crack growth properties of the base metal and weld metal of a type 304 stainless steel pipeline for LNG transmission. *Press. Vessel. Piping* **2001**, *78*, 351–357. [CrossRef]
4. Hong, S.Y.; Markus, I.; Jeong, W.-C. New cooling approach and tool life improvement in cryogenic machining of titanium alloy Ti-6Al-4V. *Int. J. Mach. Tools Manuf.* **2001**, *41*, 2245–2260. [CrossRef]
5. Zhao, X.; PAN, T.; Wang, Q.; Su, H.; Yang, C.; Yang, Q.; Zhang, Y. Effect of intercritical quenching on reversed austenite formation and cryogenic toughness in QLT-processed 9% Ni steel. *J. Iron Steel. Res. Int.* **2007**, *14*, 240–244. [CrossRef]
6. Choi, J.K.; Lee, S.-G.; Park, Y.-H.; Han, I.-W.; Morris, J.W., Jr. High Manganese Austenitic Steel for Cryogenic Applications. In Proceedings of the 22th International Offshore and Polar Engineering Conference, Rhodes, Greece, 17–22 June 2012; pp. 29–35.
7. Kim, J.-S.; Jeon, J.B.; Jung, J.E.; Um, K.-K.; Chang, Y.W. Effect of deformation induced transformation of ε-martensite on ductility enhancement in a Fe-12 Mn steel at cryogenic temperatures. *Met. Mater. Int.* **2014**, *20*, 41–47. [CrossRef]
8. Dong, Y.; Sun, Z.; Xia, H.; Feng, J.; Du, J.; Fang, W.; Liu, B.; Wang, G.; Li, L.; Zhang, X.; et al. The Influence of Warm Rolling Reduction on Microstructure Evolution, Tensile Deformation Mechanism and Mechanical Properties of an Fe-30Mn-4Si-2Al TRIP/TWIP Steel. *Metals* **2018**, *8*, 742. [CrossRef]
9. Allain, S.; Chateau, J.-P.; Bouaziz, O.; Migot, S.; Guelton, N. Correlations between the calculated stacking fault energy and the plasticity mechanisms in Fe–Mn–C alloys. *Mater. Sci. Eng. A* **2004**, *387*, 158–162. [CrossRef]
10. Curtze, S.; Kuokkala, V.-T. Dependence of tensile deformation behavior of TWIP steels on stacking fault energy, temperature and strain rate. *Acta Mater.* **2010**, *58*, 5129–5141. [CrossRef]
11. Park, B.H.; Um, H.Y.; Kim, J.G.; Jeong, H.Y.; Lee, S.; Kim, H.S. Large deformation behavior of twin-induced plasticity steels under high-pressure torsion. *Mater. Int.* **2016**, *22*, 1003–1008. [CrossRef]
12. Madivala, M.; Schwedt, A.; Prahl, U.; Bleck, W. Strain Hardening, Damage and Fracture Behavior of Al-Added High Mn TWIP Steels. *Metals* **2019**, *9*, 367. [CrossRef]
13. Idrissi, H.; Renard, K.; Schryvers, D.; Jacques, P.J. On the relationship between the twin internal structure and the work-hardening rate of TWIP steels. *Scr. Mater.* **2010**, *63*, 961–964. [CrossRef]
14. Sakai, T.; Belyakov, A.; Kaibyshev, R.; Miura, H.; Jonas, J.J. Dynamic and post-dynamic recrystallization under hot, cold and severe plastic deformation conditions. *Prog. Mater. Sci.* **2014**, *60*, 130–207. [CrossRef]
15. Karaman, I.; Sehitoglu, H.; Gall, K.; Chumlyakov, Y.I.; Maier, H.J. Deformation of single crystal Hadfield steel by twinning and slip. *Acta Mater.* **2000**, *48*, 1345–1359. [CrossRef]

16. Yuan, X.; Chen, L.; Zhao, Y.; Di, H.; Zhu, F. Influence of annealing temperature on mechanical properties and microstructures of a high manganese austenitic steel. *J. Mater. Process. Technol.* **2015**, *217*, 278–285. [CrossRef]
17. Gutierrez-Urrutia, I.; Zaefferer, S.; Raabe, D. The effect of grain size and grain orientation on deformation twinning in a Fe–22 wt.% Mn–0.6 wt.% C TWIP steel. *Mater. Sci. Eng. A* **2010**, *527*, 3552–3560. [CrossRef]
18. Shen, Y.; Qiu, C.; Wang, L.; Sun, X.; Zhao, X.; Zuo, L. Effects of cold rolling on microstructure and mechanical properties of Fe–30Mn–3Si–4Al–0.093 C TWIP steel. *Mater. Sci. Eng. A* **2013**, *561*, 329–337. [CrossRef]
19. Lee, S.-I.; Lee, S.-Y.; Han, J.; Hwang, B. Deformation behavior and tensile properties of an austenitic Fe-24Mn-4Cr-0.5 C high-manganese steel: Effect of grain size. *Mater. Sci. Eng. A* **2019**, *742*, 334–343. [CrossRef]
20. Hu, J.; Du, L.-X.; Sun, G.-S.; Xie, H.; Misra, R. The determining role of reversed austenite in enhancing toughness of a novel ultra-low carbon medium manganese high strength steel. *Scr. Mater.* **2015**, *104*, 87–90. [CrossRef]
21. Sato, S.; Kwon, E.-P.; Imafuku, M.; Wagatsuma, K.; Suzuki, S. Microstructural characterization of high-manganese austenitic steels with different stacking fault energies. *Mater. Charact.* **2011**, *62*, 781–788. [CrossRef]
22. Tewary, N.; Ghosh, S.; Bera, S.; Chakrabarti, D.; Chatterjee, S. Influence of cold rolling on microstructure, texture and mechanical properties of low carbon high Mn TWIP steel. *Mater. Sci. Eng. A* **2014**, *615*, 405–415. [CrossRef]
23. Tewary, N.; Ghosh, S.; Chatterjee, S. Effect of Annealing on Microstructure and Mechanical Behaviour of Cold Rolled Low C, High Mn TWIP Steel. *Int. J. Metall. Eng.* **2015**, *4*, 12–23.
24. Behjati, P.; Kermanpur, A.; Karjalainen, L.; Järvenpää, A.; Jaskari, M.; Baghbadorani, H.S.; Najafizadeh, A.; Hamada, A. Influence of prior cold rolling reduction on microstructure and mechanical properties of a reversion annealed high-Mn austenitic steel. *Mater. Sci. Eng. A* **2016**, *650*, 119–128. [CrossRef]
25. Kim, Y.; Kim, J.; Hwang, T.; Lee, J.; Kang, C. Effect of austenite on mechanical properties in high manganese austenitic stainless steel with two phase of martensite and austenite. *Met. Mater. Int.* **2015**, *21*, 485–489. [CrossRef]
26. Bracke, L.; Verbeken, K.; Kestens, L.; Penning, J. Microstructure and texture evolution during cold rolling and annealing of a high Mn TWIP steel. *Acta Mater.* **2009**, *57*, 1512–1524. [CrossRef]
27. Haase, C.; Kühbach, M.; Barrales-Mora, L.A.; Wong, S.L.; Roters, F.; Molodov, D.A.; Gottstein, G. Recrystallization behavior of a high-manganese steel: Experiments and simulations. *Acta Mater.* **2015**, *100*, 155–168. [CrossRef]
28. Li, C.; Ma, B.; Song, Y.; Li, K.; Dong, J. The Annealing Twins of Fe-20Mn-4Al-0.3 C Austenitic Steels during Symmetric and Asymmetric Hot Rolling. *Metals* **2018**, *8*, 882. [CrossRef]
29. Haase, C.; Barrales-Mora, L.A.; Roters, F.; Molodov, D.A.; Gottstein, G. Applying the texture analysis for optimizing thermomechanical treatment of high manganese twinning-induced plasticity steel. *Acta Mater.* **2014**, *80*, 327–340. [CrossRef]
30. Santos, D.B.; Saleh, A.A.; Gazder, A.A.; Carman, A.; Duarte, D.M.; Ribeiro, É.A.; Gonzalez, B.M.; Pereloma, E.V. Effect of annealing on the microstructure and mechanical properties of cold rolled Fe–24Mn–3Al–2Si–1Ni–0.06 C TWIP steel. *Mater. Sci. Eng. A* **2011**, *528*, 3545–3555. [CrossRef]
31. Saleh, A.A.; Gazder, A.A.; Pereloma, E.V. EBSD observations of recrystallisation and tensile deformation in twinning induced plasticity steel. *Trans. Indian Inst. Met.* **2013**, *66*, 621–629. [CrossRef]
32. Yan, J.-B.; Xie, J. Experimental studies on mechanical properties of steel reinforcements under cryogenic temperatures. *Constr. Build. Mater.* **2017**, *151*, 661–672. [CrossRef]
33. Mallick, P.; Tewary, N.; Ghosh, S.; Chattopadhyay, P.J. Effect of cryogenic deformation on microstructure and mechanical properties of 304 austenitic stainless steel. *Mater. Charact.* **2017**, *133*, 77–86. [CrossRef]
34. Bouaziz, O.; Scott, C.; Petitgand, G. Nanostructured steel with high work-hardening by the exploitation of the thermal stability of mechanically induced twins. *Scr. Mater.* **2009**, *60*, 714–716. [CrossRef]
35. Hutchinson, B.; Ridley, N. On dislocation accumulation and work hardening in Hadfield steel. *Scr. Mater.* **2006**, *55*, 299–302. [CrossRef]

36. Kalinenko, A.; Kusakin, P.; Belyakov, A.; Kaibyshev, R.; Molodov, D. Microstructure and mechanical properties of a high-Mn TWIP steel subjected to cold rolling and annealing. *Metals* **2017**, *7*, 571. [CrossRef]
37. Zhang, X.; Jiang, Z.; Li, S.; Fan, J. Effect of effective grain size and grain boundary of large misorientation on upper shelf energy in pipeline steels. *J. Wuhan Univ. Technol.* **2016**, *31*, 606–610. [CrossRef]